Journal of Nanostructure in Chemistry (2019) 9:61–76
https://doi.org/10.1007/s40097-019-0298-5

ORIGINAL RESEARCH

Exploration of catalytic performance of nano-La_2O_3 as an efficient catalyst for dihydropyrimidinone/thione synthesis and gas sensing

Vishnu Ashok Adole[1] · Thansing Bhavsing Pawar[1] · Prashant Bhimrao Koli[1] · Bapu Sonu Jagdale[1]

Received: 16 December 2018 / Accepted: 4 February 2019 / Published online: 12 February 2019

Abstract

In the present work, we report an proficient, elegant, and rapid one-pot synthesis of variety of 3,4-dihydropyrimidine-2(1*H*)-one/thione derivatives from β-dicarbonyl compounds, urea/thiourea, and various aromatic aldehydes using nano-La_2O_3 catalyst under ultrasonic irradiation. This novel synthetic strategy benefits with excellent yields, short reaction time, benign reaction conditions, clean transformation, and purification of products by non-chromatographic strategies. In addition, the synthesized nano-material was also explored as an effective gas sensor for NO_2, LPG, methyl alcohol, and ammonia. The gas-sensing properties such as selectivity and sensitivity of selected gases along with response and recovery for nano-La_2O_3 sensor are reported in this paper. In this way, conferring nano-La_2O_3 is a multifunctional catalyst not only for organic synthesis but also for gas sensing. The synthesized La_2O_3 nano-material was characterized by Fourier transform IR, powder X-ray diffraction, field-emission scanning electron microscopy, high-resolution transmission electron microscopy, energy-dispersive spectroscopy, and Brunauer–Emmett–Teller isotherm. The formation of Biginelli adducts was confirmed by Fourier transform IR, ^{1}HNMR, ^{13}CNMR, DEPT-135 (distortionless enhancement by polarization transfer spectra), and mass spectral techniques.

✉ Vishnu Ashok Adole
vishnuadole86@gmail.com

[1] Research Centre in Chemistry and PG Department of Chemistry, Loknete Vyankatrao Hiray Arts, Science and Commerce College (Affiliated to Savitribai Phule Pune University Pune), Panchavati, Nashik 422003, Maharashtra, India

Graphical abstract

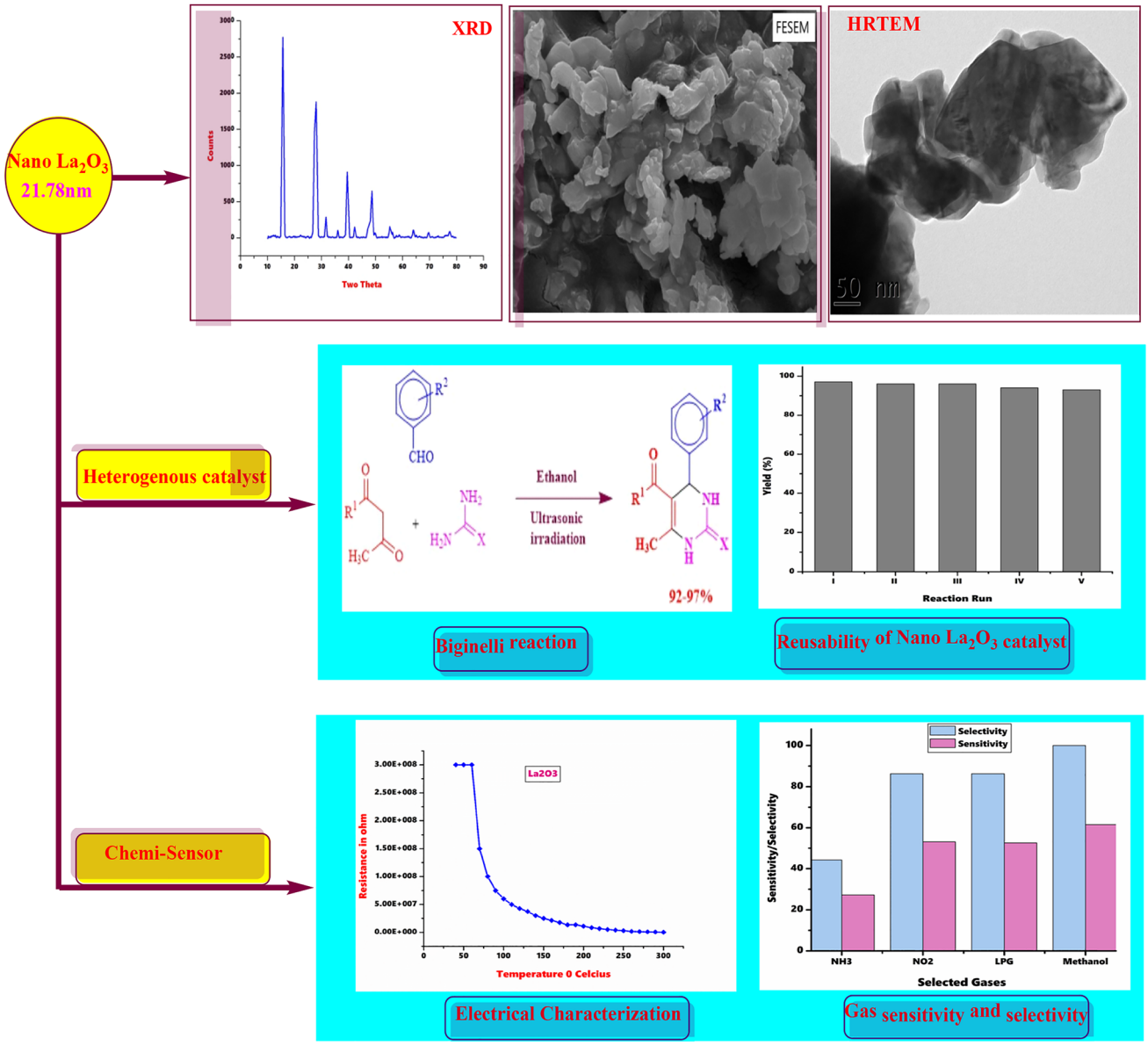

Keywords Nano-La_2O_3 catalyst · 3,4-Dihydropyrimidine-2(1*H*)-ones/thiones · Ultrasonic irradiation · Gas sensing and BET

Introduction

The most vital field of catalysis which has developed and pulled in researchers in the on-going years is derived from metal oxide nanoparticles. Metal oxide nanoparticles can catalyze large group of organic transformations on their dynamic surface and interstitial cavities [1]. An adjustment in their structures by acquainting different metal ions leads to catalysts that are exceptionally viable in higher selectivity and yield. Nowadays, the invention on metal oxide catalysts based on the principle of nano-chemistry has been notably utilized in variety of applications [2–4]. The two most crucial fields in which metal oxide nanoparticles play key role are organic synthesis and gas sensing [5, 6]. These two fields are gaining attention in terms of environment safety for both mankind and animals. Several critical issues are emerging while carrying out organic reactions using classical methods. Similarly, it is the

demanding need to monitor leakage and presence of gases in environment which are lethal to living things. By keeping this view in mind, we have focussed on development of multifunctional catalyst for green organic synthesis and real-time monitoring of gases. In the present investigation, we report nano-La_2O_3 as a benign reaction catalyst for the synthesis of dihydropyrimidinones and effective chemi-sensor.

Organic reactions that take place using metal oxide nanoparticles take place smoothly due to high surface area and presence of active adsorption sites. Variety of nano-catalysis has been employed for the synthesis of organic compounds [7–9]. At the same time, ultrasonic irradiation has been comprehensively employed in organic conversions in recent years [10]. Biginelli adducts have been found to exert promising biological properties such as calcium channel blockers [11], anti-HIV [12], antioxidant [13], anticancer [14, 15], antimicrobial [16], anti-tuberculosis [17], and anti-inflammatory activity [18]. This noteworthy medicinal profile of dihydropyrimidinones (Fig. 1) has incited the advancement of modified methodologies for Biginelli reaction. The classical version of this reaction involves the acid-catalyzed, one-pot reaction between benzaldehyde, ethyl acetoacetate, and urea in ethanol at reflux condition prompting the formation of Biginelli adduct. In the past few years, Lewis acid catalysis, solid-phase synthesis, room temperature ionic liquids microwave-assisted synthesis technique, ultrasonic-assisted organic conversion, solvent-free techniques, and some other related methods are reported [19–23]. Despite this, several reported methods have disadvantages such as use of harsh reaction conditions, elevated temperature, unsatisfactory yields, toxic catalysts and reagents, and long reaction time which are not adequate in terms of green chemistry principles (Fig. 1).

Today, the most widely recognized gas sensors are metal oxide semiconductor materials which are produced at low cost and in vast quantities. There are two fundamental types of semiconducting metal oxide sensors inclusive of n-type, whose majority carrier is electron, and p-type, whose majority carrier is hole. La_2O_3 is an excellent material with p-type semiconduction being applied in diverse applications [24–29]. Various types of pure and fabricated semiconducting materials have been found to exhibit good-to-excellent sensing responses to different hazardous and greenhouse gases [30–34]. The main object to sense these gases by various materials is to investigate the better sensing material at desired temperature. The gas sensors are particularly applicable in pollution control, to prevent industrial dangers, gas leakage protection and to make environment free from hazardous and toxic gases. In the present research, an attempt is made to sense the gases such as NH_3, NO_2, LPG, and methyl alcohol. LPG gas leakage can cause serious accidents [35]. Methanol (CH_3OH) is a central nervous system depressant and it is converted into formic acid and then formate, disturbing metabolic acidosis [36]. Inhalation of ammonia (NH_3) causes immediate burning of the nose, throat, and respiratory tract. This can lead to bronchiolar and alveolar edema causing severe respiratory problems [37]. Nitrogen dioxide (NO_2) inflames the lining of the lungs, thereby diminishing immunity to lung disorders [38]. Therefore, it becomes very essential to monitor the presence of these gases in atmosphere to avoid any hazard to humans as well as animals.

During current years, the chemistry of lanthanum compounds and their applications in organic synthesis has grown rapidly. First and foremost, because of moderate price and low toxicity makes them appealing to be used in organic transformations and other important applications. The use of lanthanide (III) compounds as catalysts in organic synthesis has pulled in incredible attention from numerous researchers. La_2O_3 is a cost effective basic materials which make them suitable for many organic reactions. Recently, lanthanum oxide has been found to be used as a recyclable catalyst for Michael addition and Hantzsch reaction. The advantages offered by synthetic ease of the catalysts and recyclability are prime significances to the advancement of heterogeneous catalytic materials. In this unique circumstance, herein, we wish to report the diverse applications of nano-La_2O_3

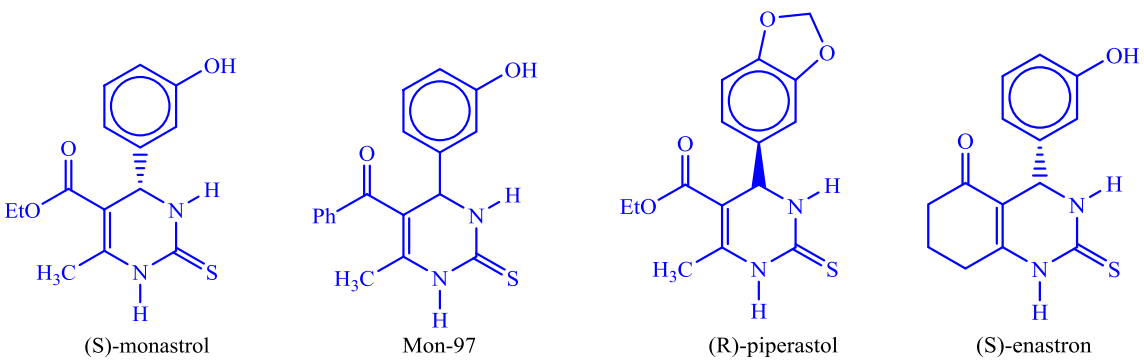

Fig. 1 Some biologically active Biginelli products

catalyst in the synthesis of Biginelli adducts and gas sensing of some flammable and hazardous gases. To the best of our insight, this is the first report on application of nano-La_2O_3 in organic synthesis under ultrasonic irradiation and gas sensing of reported gases. The advantages of the present benign protocol for the synthesis of Biginelli adducts over most of the reported strategies are short reaction time, energy efficiency, clean reaction conversion, and excellent yields. Furthermore, nano-La_2O_3 is investigated as gas sensor for the sensing of gases such as ammonia, methyl alcohol, nitrogen dioxide, and LPG. In this regard, nano-La_2O_3 is not only a proficient catalyst for Biginelli reaction under ultrasonic irradiation but also an effective gas sensor.

Materials and methods

General

Chemical reagents in high purity were purchased from SD fine chemicals and Avra synthesis and used without any further purification. ^{1}H NMR, ^{13}C NMR, and DEPT spectra were recorded with a Bruker using $CDCl_3$ and DMSO-d_6 as solvents, FT-IR spectra were obtained with potassium bromide pellets, and HRMS were recorded on Brucker with ESI as a source. The typical XRD spectrum was recorded using Bruker AXS D8 Advance, and the field-emission scanning electron microscopy (FE-SEM) spectrum was recorded using model: Nova nano-SEM 450 equipped with software xT microscope control. High-resolution transmission electron microscopy spectrum (HR-TEM) was recorded using Jeol/JEM 2100. EDS was recorded on Bruker Model: XFlash 6I30 (software: Espirit). BET was measured using instrument Autosorb iQ Station 1. Melting points were determined in open capillaries and uncorrected.

Synthesis of La_2O_3 nanoparticles

3 M solution of sodium hydroxide (NaOH) was gradually added to a solution of 1 M lanthanum (III) nitrate hexahydrate ($La(NO_3)_3{\cdot}6H_2O$) taken in a beaker. The solution is continuously stirred on magnetic stirrer during the addition of sodium hydroxide. The pH of the solution was constantly examined until it reached 12. Then, 2–3 drops of oleic acid (as a surfactant) were mixed with the solution. The resulting solution is stirred at 80 °C for a period of 4 h, and then, solution is exposed to ultrasound irradiation for 1 h. After this, solution is cooled naturally and washed several times using distilled water and ethanol to get white color precipitate. The white color precipitate was dried in oven at 110 °C and then grinded into a fine powder using mortar pestle. The fine powder obtained is then calcined for 3 h at 850 °C to obtain fine lanthanum oxide nanoparticles.

Results and discussion

X-ray diffraction (XRD) study

The XRD spectrum of La_2O_3 nanoparticles was recorded at room temperature is depicted in Fig. 2. In the XRD spectrum, it can be clearly seen that the highly narrow sharp lines for the formation of La_2O_3 nanoparticles. The Braggs reflection pattern can be assigned for the formation of lanthanum oxide with cubic phase. The intense diffraction peaks obtained from XRD data include the 2θ values 15.66, 27.31, 27.98, 31.63, 39.49, and 48.62. A strong intensity

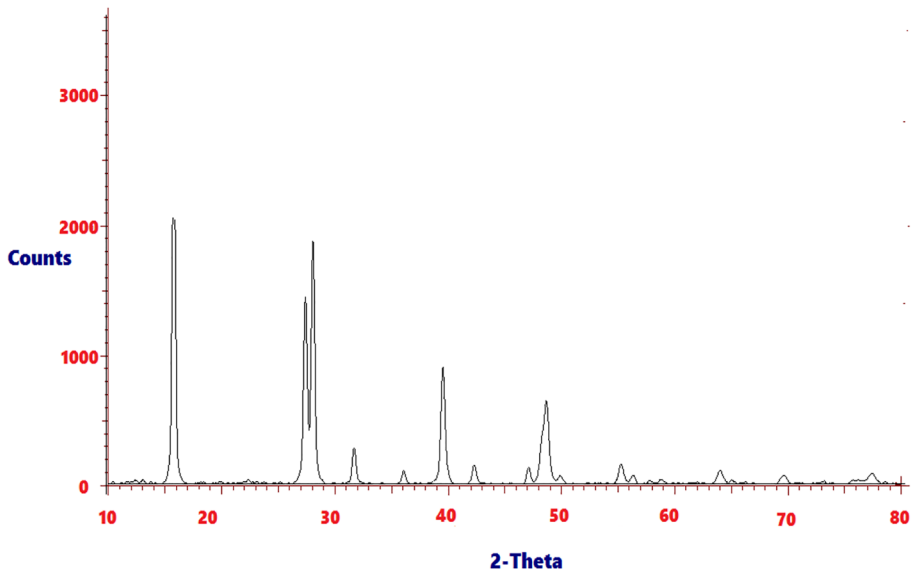

Fig. 2 XRD spectrum of prepared La_2O_3 nanoparticles calcined at 850 °C

peak (Fig. 2) is detected at a diffraction angle of 30, which is assigned to (101) plane of La_2O_3. The other peaks are assigned to (002), (102), and (110) lattice planes belonging to cubic crystalline phase of La_2O_3 (JCPDS card no. 26-0815). This outcome implies that the pure La_2O_3 crystals are successfully prepared by this method. The average particle size was calculated using Debye–Scherer's formula. [$D = K\lambda/\beta$ Cos θ], where D is average particle size, K is constant (0.9–1), β is full-width and half-maxima (FWHM) of diffracted peak, and θ is the angle of diffraction. The average particle size for lanthanum oxide nanoparticles was found to be 21.78 nm.

Field-emission scanning electron microscopy (FE-SEM)

The surface and structural morphology of prepared La_2O_3 nanoparticles was characterized by field-emission scanning electron microscopy instrument, The FE-SEM micrographs of prepared lanthanum oxide nanoparticles are depicted in Fig. 3a, b. The FE-SEM images imply agglomerated nature of lanthanum oxide nanoparticles. These nanoparticles are found to be very effective to the surface area contribution.

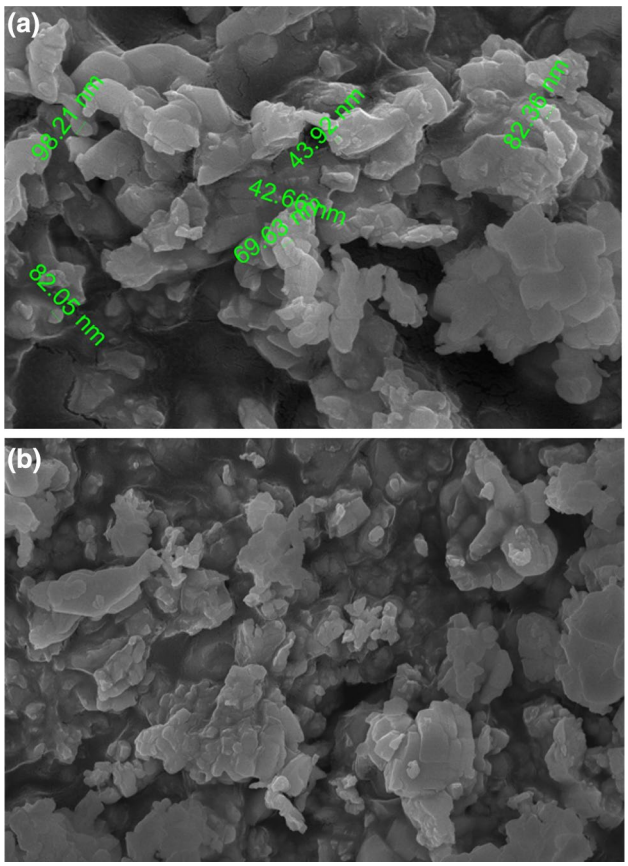

Fig. 3 **a**, **b** FE-SEM images La_2O_3 nanoparticles

The nitrogen adsorption–desorption curves (Fig. 6) also in agreement with the surface morphology found in FE-SEM images.

High-resolution transmission electron microscopy (TEM)

HR-TEM images of prepared lanthanum oxide are depicted in Fig. 4a, b. These images show the cubic crystal structure type and nanosized particles of La_2O_3 nanoparticles. The material is calcined at 850 °C; at this temperature, the La_2O_3 nanoparticles are converted to cubic crystal structure which are in agreement with the XRD results. The lanthanum oxide crystal formation is a temperature-dependent phenomenon. At lower temperature region (around 550 °C), its crystal formation is confined with the hexagonal lattice, while at the crossover range of high temperature, the cubic crystal formation is reported. From HR-TEM and FE-SEM evaluation, it has been found that the La_2O_3 nanoparticles are not correct in crystal association on account of extreme agglomeration. However, the particle size is appropriately below nanometer range to conclude that the obtained La_2O_3 is a perfect nano-material.

Energy-dispersive spectroscopy (EDS) study

The energy-dispersive spectra (EDS) was analysed for lanthanum oxide nanoparticles to confirm the elemental composition of prepared La_2O_3 nanoparticles. The EDS spectrum of La_2O_3 is illustrated in Fig. 5 clearly indicating the presence of elemental lanthanum and oxygen at 4.3 keV and 0.3 keV, respectively, which is in good agreement with the reported status of lanthanum oxide nanoparticles. The average elemental composition, atomic weight percentage of prepared La_2O_3 nanoparticles is highlighted in Table 1. In the molecular formula of lanthanum oxide, the stoichiometric atomic weight percentage for lanthanum to oxygen is 1:3, and in the present synthesis, the stoichiometric atomic weight percentage exactly matches with the ideal composition of La_2O_3 material.

Brunauer–Emmett–Teller (BET) isotherm study

Surface area is an important aspect for the important applications such as surface adsorption and gas-sensing phenomenon. The nano-La_2O_3 catalyst was investigated by nitrogen adsorption/desorption isotherm for the determining the quantitative aspects such as surface area, pore volume, and pore size determination. The typical adsorption isotherm of the La_2O_3 catalyst is shown in Figs. 6, 7. The N_2 adsorption–desorption isotherm gives the detailed idea regarding surface area (BET), pore volume, and size distribution (Table 2). By plotting the isotherm, it is found that

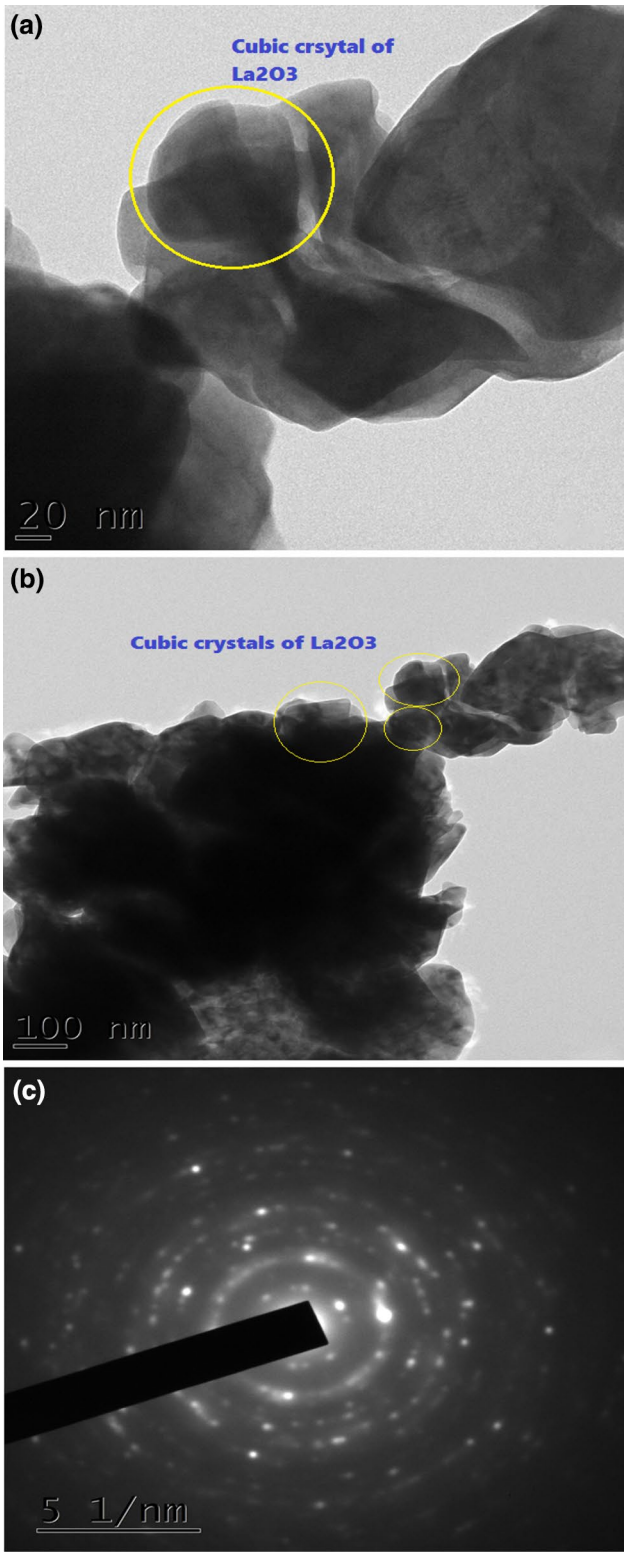

Fig. 4 **a**, **b** TEM images of La_2O_3 nanoparticles, **c** SAED pattern of La_2O_3 nanoparticles

the isotherm belongs to type IV isotherm profile with reference to the BDDT system which is a typical characteristic of porous materials.

FT-IR spectrum

In the FT-IR spectrum (Fig. 7) of lanthanum oxide nanoparticles, very weak absorption bands at 3604.96 cm^{-1} are assigned to O–H symmetric stretching vibration of water molecules which is obtained due to hygroscopic nature of lanthanum oxide. The strong absorption band at 630.72 cm^{-1} is due to La–O stretching. Hence, the existence of above-mentioned bands identifies the presence of La_2O_3.

Catalytic application of nano-La_2O_3 as a catalyst for Biginelli reaction

General procedure for the synthesis of 3,4-dihydropyrimidine-2(1*H*)-ones/thiones

The synthesized nano-material has been proficiently used as a heterogeneous catalyst for the synthesis of dihydropyrimidine-2(1*H*)-one/thione derivatives (**4a–4n**) under ultrasonic irradiation (Scheme 1). A mixture of aromatic aldehyde (10 mmol), urea/thiourea (10 mmol), ethyl acetoacetate/acetyl acetone (10 mmol), and nano-La_2O_3 (8 mol%) was mixed in a 50 ml conical flask containing ethyl alcohol as a solvent. This mixture was exposed ultrasonic irradiation at 50 °C for an appropriate time (Table 3). The mixture is then cooled to room temperature after completion of reaction (monitored by TLC). Finally, ethyl acetate was added slowly and filtered off to get extract containing crude products leaving behind nano-La_2O_3 catalyst. The extract was dried over sodium sulphate and solvent was evaporated using rotary evaporator. Pure products were obtained by further purification using ethanol. The recovered catalyst was washed with ethanol and used for five successive runs to check its reusability. The structure of all synthesized products was confirmed using spectroscopic techniques such as FT-IR, ^{1}H NMR, ^{13}C NMR, DEPT-135, and Mass spectral data.

All the experiments were performed at the optimized concentration of catalyst. For catalyst study, standard reaction between of benzaldehyde, urea, and ethyl acetoacetate was investigated (entry 4 m in Table 3). The catalyst loading was varied from 2 to 12 mol% (Table 4). By varying catalyst concentration from 2 to 12% mol%, the best outcome was obtained using concentration of 8 mol% catalyst under ultrasonic irradiation at 50 °C. Catalyst loading and selection of solvent were the important tasks during the present study. The increase in catalyst loading was found to exert substantial effect on product yield. There was not much difference in the yield and reaction

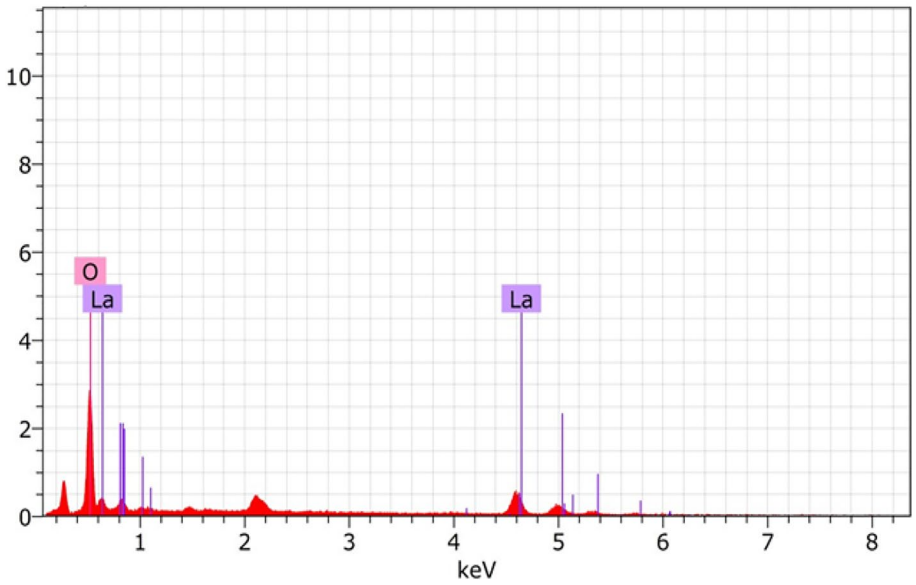

Fig. 5 EDS spectrum of La_2O_3 nanoparticles

Table 1 Elemental composition of prepared La_2O_3 nanoparticles

Element	Atomic symbol	Atomic number	Weight %	Atomic %	Weight %
Oxygen	O	8	31.65	80.08	2.78
Lanthanum	La	57	68.35	19.92	1.73

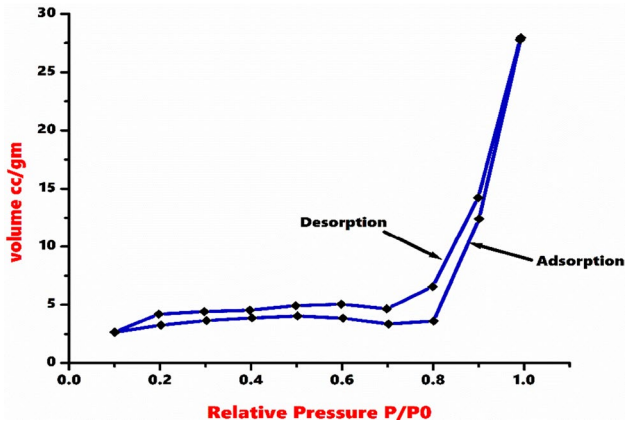

Fig. 6 N_2 adsorption–desorption isotherm for La_2O_3 nanoparticles

time when catalyst loading was changed from 8 to 10 and 12 mol%. However, in terms of catalytic efficiency, 8 mol% was found to be the better choice, and therefore, the remaining experiments were performed at the concentration of 8 mol%. From the literature survey, we found that ethanol was the most common solvent used for the dihydropyrimidinone synthesis under variety of reaction conditions, and therefore, ethanol was selected as a solvent with prime choice. During the solvent effect study, when we switched our attention to other solvents (Table 5), there was marked effect on the yield of the product. With water as a solvent, very less amount of product was obtained and with other solvents, the yield was significantly less compared to ethanol as a solvent. In case of water as a solvent, the unsatisfactory yield might be due to hygroscopic property of lanthanum oxide. The scope and generality of this protocol were studied by performing the experiments with broad range of aromatic aldehydes. Importantly, we found that benzaldehydes with variety of substitution pattern did not show large difference in the yield of 3,4-dihydropyrimidine-2(1*H*)-ones/thiones in this novel route. The substituents such as OH, Cl, OCH_3, and $N(Me)_2$ have survived which is another benefit associated with this protocol. The ultrasound irradiation disperses the agglomerated nanoparticles, thereby increasing their surface area, and also provides sufficient activation energy to reactant molecules. Henceforth, duel effect of ultrasound irradiation is observed during the course of reaction.

When we switched our attention to some previously reported catalysts to compare our findings, most of the reported methods afforded less yields with longer reaction run (Table 6). This suggests that nano-La_2O_3 catalyst under ultrasonic irradiation is more superior than most of the reported method. The probable reaction mechanism is depicted in Scheme 2 which suggests that reaction proceeds in two important stages, first aldol reaction between β-dicarbonyl compound and aromatic aldehyde and second cyclization between aldol dehydration product and urea/thiourea to furnish desired products. Importantly, the catalyst was reused for five successive runs and vitally no significant loss in its catalytic activity was found (Fig. 8 and Table 7).

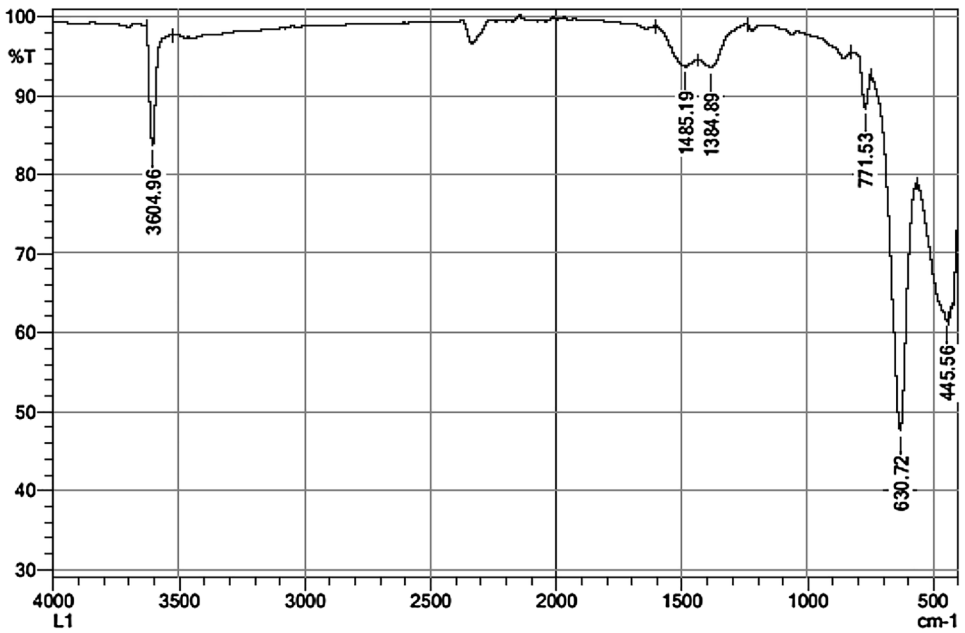

Fig. 7 FT-IR spectrum of La_2O_3 nanoparticles

Table 2 Surface area, pore volume, and pore radius obtained for La_2O_3 nanoparticles

Prepared material	Surface area (m^2/g)	Pore volume (cc/g)	Pore radius (Å)
Nano La_2O_3	11.344	0.0432	76.25

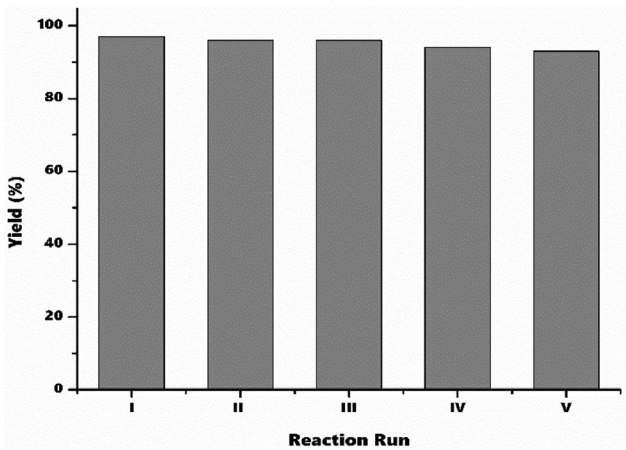

Fig. 8 Reusability of La_2O_3 nanoparticles

Spectral data of representative samples

4a-Ethyl 4-(4-isopropylphenyl)-6-methyl-2-oxo-1,2,3,4-tetrahydropyrimidine-5-carboxylate

Pale yellow crystals; m.p. 143 °C; FT-IR (cm^{-1})-3224.98, 3101.54, 2939.52, 1712.79, 1651.07, 1589.34, 1234.44, 786.96; ^{1}HNMR (400 MHz, DMSO-d6); δ (ppm)—1.17 (t, 3H) 1.22 (d, 3H), 2.32 (s, 3H), 2.87 (sept, 1H), 4.08 (q, 2H), 5.37 (d, 1H), 5.90 (s, 1H), 7.15 (d, 2H), 7.23 (d, 2H), 8.54 (s, 1H); ^{13}C NMR (100 MHz, DMSO-d6); δ (ppm) -14, 17, 24, 34, 55, 60, 101, 126, 127, 141, 146, 149, 154, 166; HRMS-(*m/z*): [M+H]—Calculated: 303.1708, Observed: 303.1704.

4b-1-(4-(4-Chlorophenyl)-6-methyl-2-thioxo-1,2,3,4-tetrahydropyrimidin-5-yl)ethan-1-one

White solid; m.p. 211 °C; FT-IR (cm^{-1})-3278.99, 3109.25, 2908.65, 1697.36, 1612.49, 1427.32, 1234.44, 786.96; ^{1}HNMR (400 MHz, DMSO-d6); δ (ppm)—2.13(s, 3H), 2.29(s, 3H), 5.24(d, J = 3.8 Hz, 1H), 7.19 (d, J = 8.4 Hz, 2H), 7.37 (d, J = 8.4 Hz, 2H), 9.75(s, 1H), 10.31(s, 1H); ^{13}C NMR (100 MHz, DMSO-d6); δ (ppm)—18.85, 31.07, 53.53, 110.85, 128.94, 129.15, 132.78, 142.33, 145.49, 174.72, 195.19; DEPT-135; δ (ppm)—18.86(CH_3), 31.07(CH_3), 53.53(CH), 128.94(Ar CH), 129.15 (Ar CH) (all up), 110.85, 132.78, 142.33, 145.49, 174.72, 195.19 (absent).

4c-Ethyl 4-(3,4-dimethoxyphenyl)-6-methyl-2-oxo-1,2,3,4-tetrahydropyrimidine-5-carboxylate

White solid; m.p. 178 °C; FT-IR (cm^{-1})—3248.13, 3093.82, 2962.66, 1627.92, 1442.75, 1226.73, 1149.57, 763.81; ^{1}HNMR (400 MHz, DMSO-d6); δ (ppm)—1.11(t, J = 7.0 Hz, 3H), 2.24(s, 3H), 3.71(s, 6H), 3.99(q, J = 7.0 Hz, 2H), 5.09(d, J = 3.8 Hz, 1H), 6.72 (dd, J = 8.2, 2.1 Hz, 1H)), 6.84 (d, J = 2.1 Hz, 1H), 6.89 (d, J = 8.2 Hz, 1H), 7.69(s, 1H), 9.16(s, 1H); ^{13}C NMR (100 MHz, DMSO-d6); δ (ppm)—14.68, 18.28, 53.96, 55.90, 56.02, 59.70, 99.86, 110.91, 112.21,

Table 3 Physicochemical data of synthesized compounds

Entry	R^1	R^2	X	Yield (%)[a]	Reaction time (min)	M.P. (°C) Found	M.P. (°C) Reported
4a	OEt	4-$CH(CH_3)_2$	O	93	55	142	143
4b	CH_3	4-Cl	S	92	40	211	211
4c	OEt	3-OCH_3, 4-OCH_3	O	92	50	179	178
4d	CH_3	3-OCH_3, 4-OCH_3	S	95	65	222	220
4e	CH_3	4-OH, 3-OCH_3	S	90	60	222	222
4f	CH_3	3-OCH_3, 4-OCH_3, 5-OCH_3	S	92	72	148	152
4g	CH_3	4-Cl	O	96	30	213	214
4h	OEt	4-OH, 3-OCH_3	O	91	80	186	188
4i	CH_3	4-$N(CH_3)_2$	S	93	40	237	238
4n	OEt	4-Cl	O	93	55	218	216
4k	CH_3	–	O	97	45	236	236
4l	CH_3	4-$N(CH_3)_2$	O	92	45	212	210
4m	OEt	–	O	97	60	206	208
4j	CH_3	4-OCH_3	O	95	48	167	166

[a]Yield refers to pure isolated products

Scheme 1 Nano-La_2O_3-catalyzed dihydropyrimidine-2(1*H*)-ones/thiones synthesis under ultrasonic irradiation

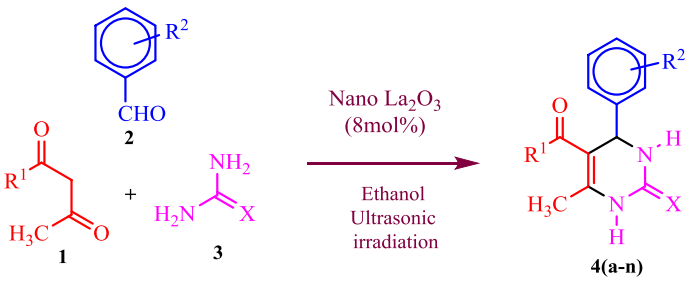

Table 4 Optimization of catalyst for the synthesis of 4 m

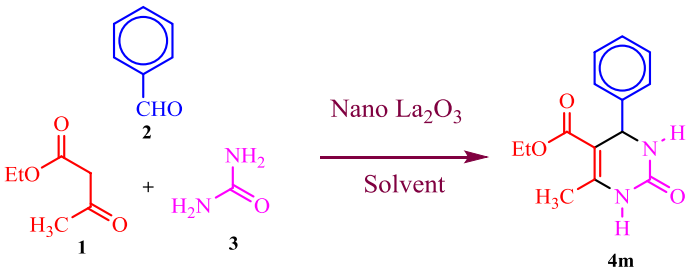

Entry	La_2O_3 catalyst (mol%)	Time (min)	Yield (%)[a]
1	–	240	Trace
2	2	150	30
3	4	60	72
4	6	60	72
5	8	50	97
6	10	55	93
7	12	55	92

Reaction conditions: benzaldehyde (10 mmol), urea (10 mmol), and ethyl acetoacetate (10 mmol) in ethanol under ultrasonic irradiation at 50 °C

[a]Isolated yield of pure product

Table 5 Solvent optimization study

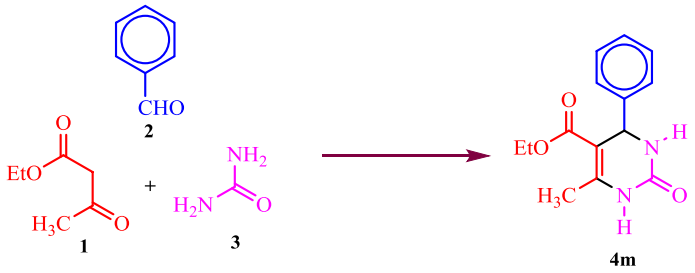

Entry	Solvent	La_2O_3 catalyst (mol%)	Time (min)	Yield (%)[a]
1	MeOH	8	60	80
2	CH_2Cl_2	8	70	70
3	DMF	8	65	60
4	MeCN	8	80	55
5	AcOH	8	90	65
6	H_2O	8	100	20
7	$PhCH_3$	8	90	30
8	THF	8	70	40
9	CCl_4	8	70	25
10	EtOH	8	50	97

Reaction conditions: benzaldehyde (10 mmol), urea (10 mmol), ethyl acetoacetate (10 mmol), and nano-La_2O_3 (8 mol %) under ultrasonic irradiation at 50 °C

[a]Isolated yield of pure product

Table 6 Comparison of catalytic performance of nano-La_2O_3 with other reported works

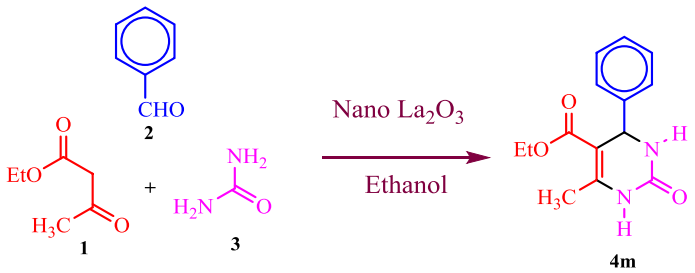

Entry	Solvent	Catalyst	Time (min)	Reaction condition	Yield (%)	References
1	Acetic acid	$H_3PMo_{12}O_{40}$	360	Reflux	80	[39]
2	Ethanol	$Cu(OTf)_2$	720	80 °C	85	[40]
3	Solvent free	$P(Ph)_3$	600	100	70	[41]
4	Ethanol	Calixarene 7	480	Reflux	69	[42]
5	Solvent free	H_2SO_4-Silica	120	55 °C	80	[43]
6	Ethanol	Trichloroisocyanuric acid (TCCA)	720	Reflux	94	[44]
7	Dioxane and Isopropanol	PS-PEG-SO_3H	600	80	86	[45]
8	EtOH	Nano La_2O_3	50	50 °C	97	Present study

Scheme 2 Plausible catalytic cycle

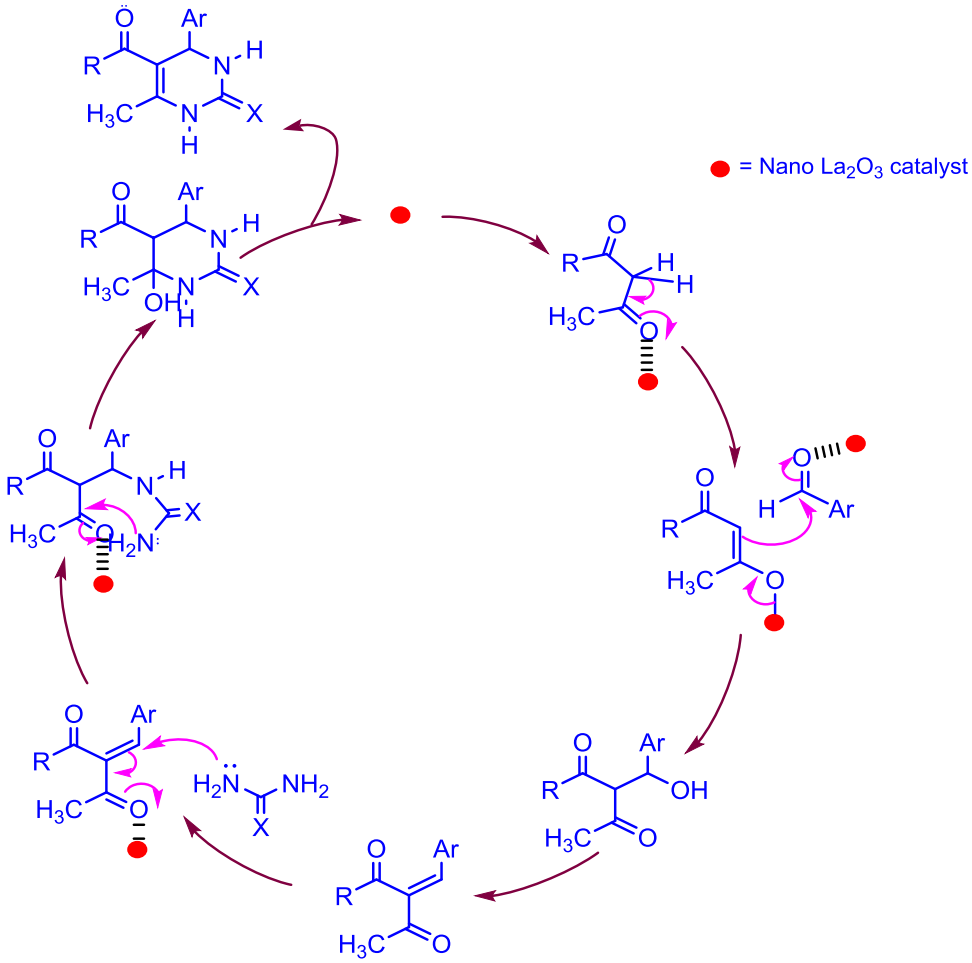

118.38, 137.84, 148.53, 148.68, 148.95, 152.77, 165.94; DEPT-135; δ (ppm)—14.68 (CH_3), 18.28 (CH_3), 53.97 (CH), 55.90 (OCH_3), 56.02 (OCH_3), 110.90 (Ar CH), 112.20 (Ar CH), 118.38 (Ar CH) (all up), 59.70 (OCH_2) (down), 137.84, 148.53, 148.68, 148.95, 152.77, 165.94 (all absent); MASS—(*m/z*): 320 ($M^{+\cdot}$), 291, 273, 247, 183.

4d-1-(4-(3,4-Dimethoxyphenyl)-6-methyl-2-thioxo-1,2,3,4-tetrahydropyrimidin-5-yl)ethan-1-one

Yellow solid; m.p. 220 °C; FT-IR (cm^{-1})—3332.99, 3232.70, 3109.25, 2924.09, 1681.93, 1635.64, 1458.18, 1219.01, 1087.85, 771.53; ^{1}HNMR (400 MHz, DMSO-d6); δ (ppm)—1.9 (s, 3H), 2.1(s, 3H), 3.74 (s, 3H), 3.75 (s, 3H), 5.24 (d, $J = 3.76$ Hz, 1H), 6.7 (m, 1H)), 6.9 (m, 2H), 9.64 (d, 1H), 10.18 (s, 1H); HRMS—(*m/z*): [M+H]—Calculated: 307.1116, Observed: 307.1115.

Table 7 Reusability of nano-La_2O_3 catalyst for Biginelli reaction

Run	I	II	III	IV	V
Yield	97	96	96	94	93

4e-1-(4-(4-Hydroxy-3-methoxyphenyl)-6-methyl-2-thioxo-1,2,3,4-tetrahydropyrimidin-5-yl)ethan-1-one

Off white solid; m.p. 222 °C; FT-IR (cm^{-1})—3533.59, 3240.41, 3109.25, 2931.80, 1697.36, 1643.35, 1512.19, 1435.04, 1219.01, 786.96; ^{1}HNMR (400 MHz, DMSO-d6); δ (ppm)—2.10 (s, 3H), 2.33 (s, 3H), 3.77 (s, 3H), 5.22 (s, 1H), 6.61 (d, $J = 8.0$ Hz, 1H)), 6.72 (d, $J = 8.0$ Hz, 1H), 6.86 (s, 1H), 8.93 (s, 1H), 9.60 (s, 1H), 10.15 (s, 1H); ^{13}C NMR (100 MHz, DMSO-d6); δ (ppm)—17.94, 29.81, 53.79, 55.36, 59.88, 109.83, 111.01, 115.12, 118.63, 133.61, 143.82, 146.05, 147.28, 173.53, 194.70.

4f-1-(6-Methyl-2-thioxo-4-(3,4,5-trimethoxyphenyl)-1,2,3,4-tetrahydropyrimidin-5-yl)ethan-1-one

Yellow solid; m.p. 152 °C; FT-IR (cm^{-1})—3282.76, 3208.28, 3097.29, 2922.29, 1695.03, 1614.24, 1486, 1260, 833.88, 789.62; ^{1}HNMR (400 MHz, DMSO-d6); δ (ppm)—2.17 (s, 3H), 2.35 (s, 3H), 3.66 (s, 3H), 3.75 (s, 6H), 5.28 (d, $J = 3.76$ Hz, 1H), 6.54 (s, 1H)), 6.9 (m, 2H), 9.66 (s, 1H),

10.24 (s, 1H); ^{13}C NMR (100 MHz, DMSO-d6); δ (ppm)—18.13, 30.18, 53.91, 55.72, 59.88, 103.76, 109.95, 137.02, 138.29, 144.40, 152.86, 174.09, 194.76; MASS—(*m/z*): 336 ($M^{+\cdot}$), 305, 169, 43.

4g-5-Acetyl-4-(4-chlorophenyl)-6-methyl-3,4-dihydropyrimidin-2(1H)-one

White solid; m.p. 214 °C; FT-IR (cm^{-1})—3219.67, 3099.83, 2978.50, 1699.53, 1644.01, 1572.86, 1485.99, 1287.25, 865.98; ^{1}HNMR (400 MHz, DMSO-d6); δ (ppm)—2.17(s, 3H), 2.35(s, 3H), 5.30(d, $J=3.88$ Hz, 1H), 7.25 (m, 2H), 7.19 (m, 2H), 9.73(d, 1H), 10.30(s, 1H); ^{13}C NMR (100 MHz, DMSO-d6); δ (ppm)—18.29, 30.36, 53.16, 110.21, 128.31, 128.41, 132.35, 141.65, 144.72, 174.20, 194.34.

4h-Ethyl 4-(4-hydroxy-3-methoxyphenyl)-6-methyl-2-oxo-1,2,3,4-tetrahydropyrimidine-5-carboxylate

White crystals; m.p. 188 °C; FT-IR (cm^{-1})—3626.17, 3332.99, 3101.54, 2939.52, 1712.79, 1651.07, 1589.34, 1435.04, 1234.44, 1126.43, 786.96; ^{1}HNMR (400 MHz, DMSO-d6); δ (ppm)—1.07 (t, $J=7.1$ Hz, 3H). 2.19(s, 3H), 3.95 (q, $J=7.1$ Hz, 2H), 6.75 (d, $J=2.0$ Hz, 1H), 5.01 (d, $J=3.2$ Hz, 1H), 6.66 (d, $J=8.2$ Hz, 1H), 6.56 (dd, $J=8.2$, 2.0 Hz, 1H), 8.87 (s, 1H), 9.08 (s, 1H); ^{13}C NMR (100 MHz, DMSO-d6); δ (ppm)—14.68, 18.26, 54.06, 56.05, 59.65, 100.04, 111.35, 115.78, 118.78, 136.43, 146.29, 147.75, 148.44, 152.76, 165.97; DEPT-135; δ (ppm)—14.68 (CH_3), 18.27 (CH_3), 54.06 (CH), 56.05 (OCH_3), 111.34 (Ar CH), 115.77 (Ar CH), 118.78 (Ar CH) (all up), 59.65 (OCH_2) (down), 136.43, 146.29, 147.75, 148.44, 152.76, 165.97 (all absent).

4i-1-(4-(4-(Dimethylamino)phenyl)-6-methyl-2-thioxo-1,2,3,4-tetrahydropyrimidin-5-yl)ethan-1-one

Orange solid; m.p. 238 °C; FT-IR (cm^{-1})—3219.67, 3099.83, 2978.50, 1699.53, 1644.01, 1572.86, 1485.99, 1287.25, 862.98; ^{1}HNMR (400 MHz, DMSO-d6); δ (ppm)—2.24 (s, 3H), 2.86 (s, 6H), 3.53 (s, 3H), 5.06 (d, $J=3.2$ Hz, 1H), 6.62 (d, $J=8.0$ Hz, 2H), 7.06 (d, $J=8.0$ Hz, 2H), 7.54 (s, 1H), 9.06 (s, 1H); HRMS—(*m/z*): [M+H]—Calculated: 290.1504, Observed: 290.1503.

4j-Ethyl 4-(4-chlorophenyl)-6-methyl-2-oxo-1,2,3,4-tetrahydropyrimidine-5-carboxylate

Cream color solid; m.p. 216 °C; FT-IR (cm^{-1})—3279.93, 3175.21, 3114.76, 2992.07, 1730.37, 1706.86, 1620.09, 1576.84, 1456.75, 1252.03, 828.86; ^{1}HNMR (400 MHz, DMSO-d6); δ (ppm)—1.13 (t, $J=7$ Hz, 3H), 2.28 (s, 3H), 4.00 (q, $J=7$ Hz, 2H), 5.20 (d, $J=3.16$ Hz, 1H), 7.26 (m, 4H), 7.72 (s, 1H), 9.20 (s, 1H).

Application of La_2O_3 as a gas sensor

Preparation of La_2O_3 sensor by screen-printing method

The nano-La_2O_3 paste used in screen printing was prepared by maintaining the inorganic-to-organic materials ratio at 7:3. The inorganic part consists of a functional material nano-La_2O_3. The organic part consists of 8% ethyl cellulose (EC) and 92% butyl carbitol acetate (BCA). The nano-La_2O_3 powder (0.7 g) along with ethyl cellulose (EC) was mixed thoroughly in an acetone medium with mortar and pestle. A solution of BCA which was added dropwise until proper thixotropic properties of the paste were achieved. Nano-La_2O_3 thick films were prepared on glass substrate using standard screen-printing technique. The films were dried under IR radiation for 45 min to remove the organic vehicle and then fired at temperature 400 °C for 5 h in muffle furnace.

Electrical characterization and gas-sensing study of La_2O_3 nano-catalyst

The gas-sensing properties of La_2O_3 thick films was examined at different elevated temperatures from 350 °C to room temperature. The electrical resistance of the thick film sensor was measured in the absence of any other gases in the glass-domed chamber. The typical semiconducting nature

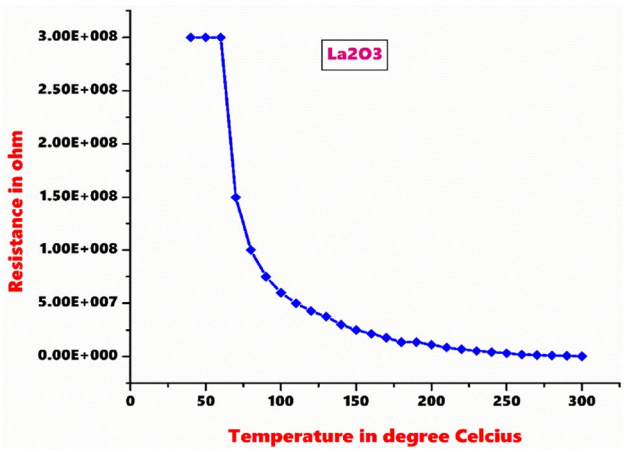

Fig. 9 Electrical characterization La_2O_3 nanoparticles

Table 8 Summary of response and recovery for La_2O_3 sensor of methyl alcohol vapours

Name of the gas	Maximum response (%)	Response time (s)	Recovery time (s)
CH_3–OH	63	20	42

of lanthanum oxide thick film is shown in Fig. 9, wherein continuous decrease in temperature, the change in resistance of the film was recorded. Resistance increases at the initial stage in low-temperature region, and with a progression of temperature, resistance decreases in a high-temperature region to document a semiconducting behaviour of the La_2O_3 oxide.

The gas-sensing performance was measured by static gas sensor assembly. The DC resistance of the thick films of La_2O_3 thick film sensor was measured using traditional half bridge method, at the series of elevated temperatures. The film was fixed at the base of gas-sensing assembly, wherein Chromel–Alumel thermocouple was firmly fixed to sense the temperature of the thick film sensor. The temperature sensed by thermocouple was digitally recorded with the aid of temperature recorder (model number PEW-202/PEW-205). The gases selected for the sensing purpose were brought within the chamber with the help of inlet metallic pipe. The DC voltage was applied to the circuit, and simultaneously, resistance of the film was recorded by digital millimetre (model number CIE Classic 5175). Each cycle of the gas introduced inside the glass chamber was pulled back by lifting the glass chamber and settled temperature was provided to evacuate the gas build-up of the film. The oxygenated air was permitted through the chamber at every gas affectability cycle. The electrical resistance of the thick films in the presence of air (Ra), as well as in the presence of gas (Rg) was measured to calculate the gas response or sensitivity (S) which is given by Eq. 1:

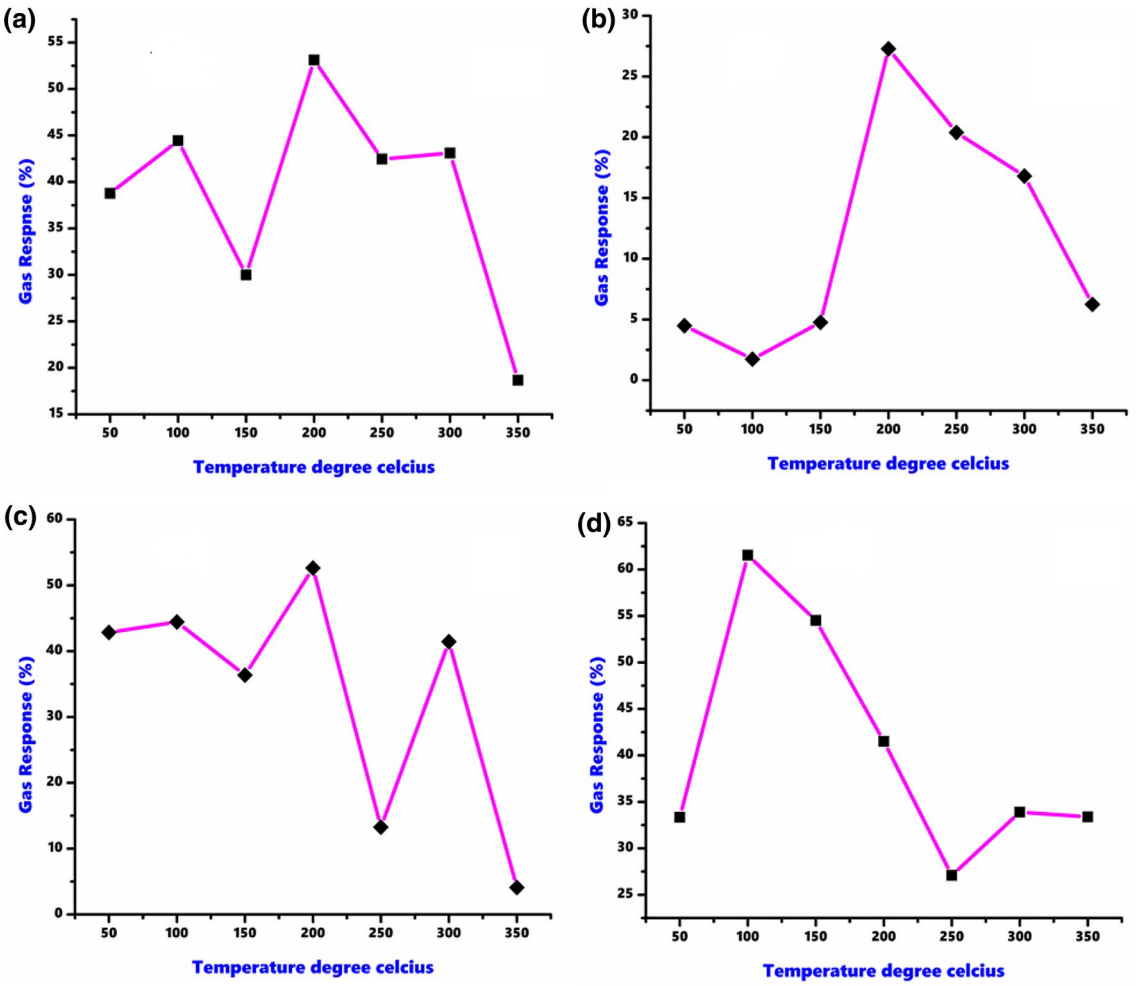

Fig. 10 Gas response (sensitivity) curves of Lanthanum oxide sensor for **a** NO_2, **b** NH_3, **c** LPG, and **d** methyl alcohol

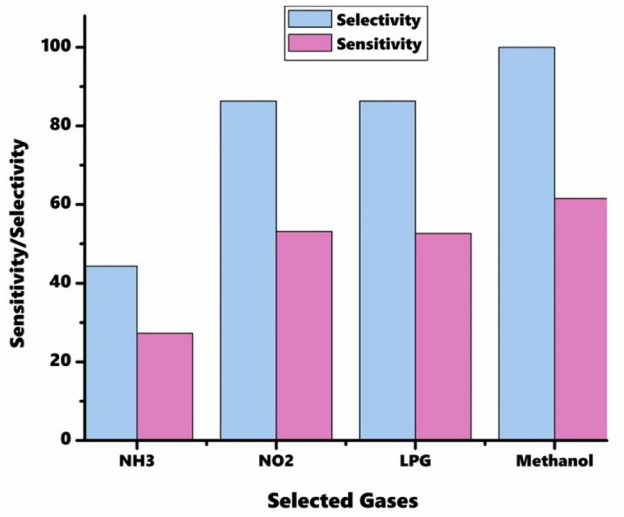

Fig. 11 Sensitivity and selectivity for NH_3, NO_2, LPG, and methyl alcohol for La_2O_3 sensor

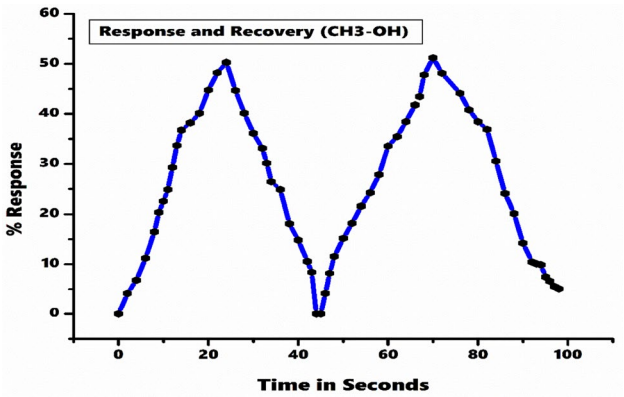

Fig. 12 Response and recovery

$$S\% = \mathrm{Ra} - \mathrm{Rg}/\mathrm{Ra} \times 100. \quad (1)$$

The sensing of gases NH_3, LPG, NO_2, and CH_3OH of 500 ppm concentrations has been examined at temperature of 50–350 °C. The electrical resistance, selectivity, sensitivity, and response–recovery time were measured for the thick film of lanthanum oxide sensor (Table 8).

Sensitivity and selectivity of lanthanum oxide sensor

The sensitivity of selected gases (500 ppm concentration) against temperature (50–350 °C) is shown in Fig. 10 and the compared selectivity of these gases is shown in Fig. 11. The sensitivity and selectivity can be calculated by applying the temperature to the particular sensor for the sensing of particular gas. The data obtained from methyl alcohol gas-sensing study indicate that the maximum response is 63% at 100 °C. Previously reported response for methanol gas using lanthanum oxide sensor was 60% at higher temperature reported by Yue Gao [50]. On the other hand, the response showed by La_2O_3 sensor for LPG, NH_3, and NO_2 was found to be 55%, 27%, and 53%, respectively, at the temperature 200 °C. The gas response reported in the present work is found to be more significant in comparison with the previous reported data. The selectivity data presented in Fig. 11 indicate that all the gases are found to show good-to-excellent selectivity for lanthanum oxide sensor. The response and recovery is depicted in Fig.12. For gases LPG, methyl alcohol, and NO_2, the selectivity is over 80% (Table 9). When we compared our methanol gas-sensing results with some the reported data (Table 10), it can be clearly seen that methanol gas sensing reported herein is not only fantastic, but also observed at little lower temperature. This gives idea about better sensing potential of lanthanum oxide nano-material reported herein. Thus, by keen observation, on the basis of sensing response and selectivity data, we can conclude that nano-La_2O_3 can be effectively applied as gas sensor for these gases.

Conclusions

In summary, catalytic performance of the nano-La_2O_3 was explored in Biginelli reaction for the one-pot synthesis of 3,4-dihydropyrimidine-2(1*H*)-one/thione derivatives under ultrasonic irradiation and it was found that the present method has brilliant efficiency in the synthesis of Biginelli adducts. Short reaction time, use of economical, non-toxic and green catalyst and clean reaction conversion with magnificent yields are the key highlights of the protocol revealed

Table 9 Summary of the gas response and selectivity of La_2O_3 sensor for selected gases

Entry	Gases (500 ppm)	Response (%)	Selectivity (%)	Maximum response temperature (°C)
1	CH_3-OH	63	100	100
2	LPG	55	86.33	200
3	NH_3	27	44.30	200
4	NO_2	53	86.33	200

Table 10 Comparison of methyl alcohol gas-sensing performance of La_2O_3 nano-material with reported methods

Entry	Material	Method of preparation of sensor	Type of sensor	Sensing temperature (°C)	Gas concentration (ppm)	Reported sensitivity (%)	References
1	Ag–$LaFeO_3$	Sol–gel	Thin film	195	5	42	[46]
2	SnO_2	Sol–gel	Thin film	280	1000	22	[47]
3	Nb–TiO_2	Sol–gel	Thin film	300	400	14	[48]
4	$LaFeO_3$	Sol–gel	Thick film	150	500	60	[49]
5	Au–ZnO	Hydrothermal	Thick	440	100	5	[50]
6	ZnO	Hydrothermal	Thick	150	50	35	[51]
7	La_2O_3	Co-precipitation	Thick film	100	500	63	Present study

in this and, therefore, renders this elegant protocol environmentally suitable synthetic methodology for the Biginelli reaction. In addition, nano-La_2O_3 was also explored as gas sensor for four different gases showing better sensitivity and selectivity to flammable and toxic methyl alcohol. The response and recovery are found to be very effective for the toxic methanol gas as compared to the previous reports. In this context, nano-La_2O_3 is not only an efficient catalyst for Biginelli reaction under ultrasonic irradiation, but also an effective gas sensor, thereby presenting its multifunctional character.

Acknowledgements Authors are grateful to acknowledge CIF, Savitribai Phule Pune University, Pune and SAIF, Punjab University, Chandigarh for SEM, EDS, NMR, and mass spectral analysis, STIC, Cochin University, Kerala for XRD and TEM analysis. Authors are also thankful to the Lokenete Vyankatrao Hiray Arts, Science and Commerce College Panchavati, Nashik for providing research facilities.

References

1. Schauermann, S., Nilius, S., Shaikhutdinov, S., Freund, H.J.: Nanoparticles for heterogeneous catalysis: new mechanistic insights. Acc. Chem. Res. **46**(8), 1673–1681 (2013)
2. Chaturvedi, S., Dave, P.N., Shah, N.K.: Applications of nano-catalyst in new era. J. Saudi Chem. Soc. **16**, 307–325 (2012)
3. Shan, S., Yan, S., Tyagi, R.D., Surampalli, R.Y., Zhang, T.C.: Applications of nanomaterials in environmental science and engineering: review. Pract. Period Hazard Toxic Radioact Waste Manag **13**, 110–119 (2009)
4. Sharma, N., Ojha, H., Bharadwaj, A., Pathak, D., Sharma, R.: Preparation and catalytic applications of nanomaterials: a review. RSC Adv. **5**, 53381–53403 (2015)
5. Astruc, D., Lu, F., Aranzaes, J.R.: Nanoparticles as recyclable catalysts: the frontier between homogeneous and heterogeneous catalysis. Angew. Chem. Int. Ed. **44**, 7852–7872 (2015)
6. Xu, K., Fu, C., Gao, Z., Wei, F., Ying, Y., Xu, C., Fu, G.: Nanomaterial-based gas sensors: a review. Instrum Sci Technol **46**, 115–145 (2018)
7. Datsan, A., Kulkarni, A., Torok, B.: Environmentally benign synthesis of heterocyclic compounds by combined microwave-assisted heterogeneous catalytic approaches. Green Chem. **14**, 17–37 (2012)
8. Kassaee, M.Z., Rostamizadeh, S., Shadjou, N., Motamedi, E., Esmaeelzadeh, M.: An efficient one-pot solvent-free synthesis of 2,3-dihydroquinazoline-4(1H)-ones via Al/Al_2O_3 nanoparticles. J Heterocycl Chem **47**, 1421–1424 (2010)
9. Maleki, B., Mofrada, A.V., Tayebee, R., Khojastehnezhad, A., Alinezhad, H., Rezaei Seresht, E.: One-pot synthesis of 1,4-dihydropyridine derivatives catalyzed by silica-coated magnetic $NiFe_2O_4$ nanoparticles-supported $H14[NaP_5W_{30}O_{110}]$. Russ. J. Gen. Chem. **87**, 2922–2929 (2017)
10. Draye, M., Kardos, N.: Advances in green organic sonochemistry. Top. Curr. Chem. **374**, 74 (2016)
11. Atwal, K.S., Rovnyak, G.C., Schwartz, J., Moreland, S., Hedberg, A., Gougoutas, J.Z., et al.: Dihydropyrimidine calcium channel blockers: 2-heterosubstituted 4-aryl-1,4-dihydro-6-methyl-5- pyrimidinecarboxylic acid esters as potent mimics of dihydropyridines. J. Med. Chem. **33**(9), 1510–1515 (1990)
12. Kim, J., Park, C., Ok, T., So, W., Jo, M., Seo, M., et al.: Discovery of 3,4-dihydropyrimidin-2(1H)-ones with inhibitory activity against HIV-1 replication. Bioorg. Med. Chem. Lett. **22**(5), 2119–2124 (2012)
13. Mansouri, M., Movahedian, A., Rostami, M., Fassihi, A.: Synthesis and antioxidant evaluation of 4-(furan-2-yl)-6-methyl-2-thioxo-1,2,3,4-tetrahydropyrimidine-5-carboxylate esters. Res Pharm Sci **7**(4), 257–264 (2012)
14. Kumar, B.R.P., Sankar, G., Baig, R.B.N., Chandrashekaram, S.: Novel Biginelli dihydropyrimidines with potential anticancer activity: a parallel synthesis and CoMSIA study. Eur. J. Med. Chem. **44**(10), 4192–4198 (2009)
15. Yadlapalli, R.K., Chourasia, O.P., Vemuri, K., Sritharan, M., Perali, R.S.: Synthesis and in vitro anticancer and antitubercular activity of diarylpyrazole ligated dihydropyrimidines possessing lipophilic carbamoyl group. Bioorg. Med. Chem. Lett. **22**(8), 2708–2711 (2012)
16. Sharma, P., Rane, N., Gurram, V.K.: Synthesis and QSAR studies of pyrimido[4,5 d]pyrimidine-2,5-dione derivatives as potential antimicrobial agents. Bioorg. Med. Chem. Lett. **14**, 4185–4190 (2004)
17. Trivedi, A.R., Bhuva, V.R., Dholariya, B.H., Dodiya, D.K., Kataria, V.B., Shah, V.H.: Novel dihydropyrimidines as a potential new class of antitubercular agents. Bioorg. Med. Chem. Lett. **20**(20), 6100–6102 (2010)
18. Tale, R.H., Rodge, A.H., Hatnapure, G.D., Keche, A.P.: The novel 3,4-dihydropyrimidin-2(1H)-one urea derivatives of N-aryl urea: synthesis, anti-inflammatory, antibacterial and antifungal activity evaluation. Bioorg. Med. Chem. Lett. **21**, 4648–4651 (2011)
19. Adibi, H., Samimi, H.A., Beygzadeh, M.: Iron(III) trifluoroacetate and trifluoromethanesulfonate: recyclable Lewis acid catalysts

for one-pot synthesis of 3,4-dihydropyrimidinones or their sulfur analogues and 1,4-dihydropyridines via solvent-free Biginelli and Hantzsch condensation protocols. Catal. Commun. **8**, 2119–2124 (2007)
20. Hamper, B.C., Gan, K.Z., Owen, T.J.: Solid phase synthesis of dihydropyrimidinones and pyrimidinone carboxylie acids from malonic acid resin. Tetrahedron Lett. **40**, 4973–4976 (1999)
21. Fang, D., Luo, J., Zhou, X., Ye, Z., Liu, Z.: One-pot green procedure for Biginelli reaction catalyzed by novel task-specific room-temperature ionic liquids. J. Mol. Catal. A Chem. **274**, 208–211 (2007)
22. Khabazzadeh, H., Saidi, K., Sheibani, H.: Microwave-assisted synthesis of dihydropyrimidin-2(1H)-ones using graphite supported lanthanum chloride as a mild and efficient catalyst. Bioorg. Med. Chem. Lett. **18**, 278–280 (2008)
23. Kamali, M., Shockravi, A., Doost, M.S., Hooshmand, S.E.: One-pot, solvent-free synthesis via Biginelli reaction: catalyst-free and new recyclable catalysts. Cogent Chem. **1**, 1081667 (2015)
24. Auroux, A., Artizzu, P., Ferino, I., Monaci, R., Rombi, E., Solinas, V., Petrini, G.: Dehydration of 4-methylpentan-2-ol over lanthanum and cerium oxides. J. Chem. Soc. Faraday Trans. **92**, 2619–2624 (1996)
25. Liu, J., Wang, G., Lu, L., Guo, Y., Yang, L.: Facile shape-controlled synthesis of lanthanum oxide with different hierarchical micro/nanostructures for antibacterial activity based on phosphate removal. RSC Adv. **7**, 40965–40972 (2017)
26. Rao, C.R.N., Karthikeyan, J.: Removal of fluoride from water by adsorption onto lanthanum oxide. Water Air Soil Pollut. **223**, 1101–1114 (2012)
27. Vignolo, M.F., Duhalde, S., Bormioli, M., Quintana, G., Cervera, M., Tocho, J.: Structural and electrical properties of lanthanum oxide thin films deposited by laser ablation. Appl. Surf. Sci. **197–198**, 522–526 (2002)
28. Qaroush, A.K., Alsoubani, F.A., Al-Khateeb, A.M., Nabih, E., Al-Ramahi, E., Khanfar, M.F., Assaf, K.I., Eftaiha, A.F.: An efficient atom-economical chemoselective CO_2 cycloaddition using lanthanum oxide/tetrabutyl ammonium bromide. Sustain. Energy Fuels **2**, 1342–1349 (2018)
29. Pisecny, P., Husekova, K., Frohlich, K., Harmatha, L., Soltys, J., Machajdik, D., Espinos, J.P., Jergel, M., Jakabovic, J.: Growth of lanthanum oxide films for application as a gate dielectric in CMOS technology. Mater. Sci. Semicond. Process. **7**, 231–236 (2004)
30. Dey, R., Rai, V.: Yb^{3+} sensitized Er^{3+} doped La_2O_3 phosphor in temperature sensors and display devices. Dalton Trans. **43**, 111–118 (2014)
31. Dey, A.: Semiconductor metal oxide gas sensors: a review. Mater. Sci. Eng. B **229**, 206–217 (2018)
32. Fine, G.F., Cavanagh, L.M., Afonja, A., Binions, R.: Metal oxide semi-conductor gas sensors in environmental monitoring. Sensors **10**, 5469–5502 (2010)
33. Wetchakuna, K., Samerjaia, T., Tamaekonga, N., Liewhirana, C., Siriwonga, C., Kruefua, V., Wisitsoraatb, A., Tuantranontb, A., Phanichphanta, S.: Semiconducting metal oxides as sensors for environmentally hazardous gases. Sens. Actuators B **160**, 580–591 (2011)
34. Gao, F., Qin, G.H., Li, Y.H., Jiang, Q.P., Luo, L., Zhao, K., Liu, Y.J., Zhao, H.Y.: One-pot synthesis of La-doped SnO_2 layered nanoarrays with enhanced gas-sensing performance toward acetone. RSC Adv. **6**, 10298–10310 (2016)
35. Nivolianitou, Z., Konstandinidou, M., Michalis, C.: Statistical analysis of major accidents in petrochemical industry notified to the major accident reporting system (MARS). J. Hazard. Mater. **137**, 1–7 (2006)
36. Holt, N.R., Nickson, C.P.: Severe methanol poisoning with neurological sequelae: implications for diagnosis and management. Intern. Med. J. **48**, 335–339 (2018)
37. Pyatt, F.B.: Potential effects on human health of an ammonia rich atmospheric environment in an archaeologically important cave in Southeast Asia. Occup. Environ. Med. **60**, 986–988 (2003)
38. Petit, P.C., Fine, D.H., Vásquez, G.B., Gamero, L., Slaughter, M.S., Dasse, K.A.: The pathophysiology of nitrogen dioxide during inhaled nitric oxide therapy. ASAIO **63**, 7–13 (2017)
39. Heravi, M.M., Bakhtiari, K., Bamoharram, F.F.: 12 Molybdophosphoric acid: a recyclable catalyst for the synthesis of Biginelli-type 3,4-dihydropyrimidine-2(1H)-ones. Catal. Commun. **7**, 373–376 (2006)
40. Pasunooti, K.K., Chai, H., Jensen, C.N., Gorityala, B., Wang, S., Liu, X.W.: A microwave-assisted, copper-catalyzed three-component synthesis of dihydropyrimidinones under mild conditions. Tetrahedron Lett **52**, 80–84 (2011)
41. Debache, A., Amimour, M., Belfaitah, A., Rhouati, S., Carboni, B.: A one-pot Biginelli synthesis of 3,4-dihydropyrimidin-2-(1H)-ones/thiones catalyzed by triphenylphosphine as Lewis base. Tetrahedron Lett. **49**, 6119–6121 (2008)
42. Silva, D.L., Fernandes, S.A., Sabino, A.A., Fatima, A.: *p*-Sulfonic acid calixarenes as efficient and reusable organocatalysts for the synthesis of 3,4- dihydropyrimidin-2(1H)-ones/thiones. Tetrahedron Lett. **52**, 6328–6330 (2011)
43. Pourmousavi, S.A., Hasani, M.: H_2SO_4-Silica catalyzed one-pot and efficient synthesis of dihydropyrimidones under solvent-free conditions. E J. Chem. **8**(S1), 462–466 (2011)
44. Bigdeli, M.A., Jafari, S., Mahdavinia, G.H., Hazarkhani, H.: Trichloroisocyanuric acid, a new and efficient catalyst for thesynthesis of dihydropyrimidinones. Catal. Commun. **8**, 1641–1644 (2007)
45. Quan, Z.J., Da, Y.X., Zhang, Z., Wang, X.C.: PS–PEG–SO3H as an efficient catalyst for 3,4-dihydropyrimidones via Biginelli reaction. Catal. Commun. **10**, 1146–1148 (2009)
46. Rong, Q., Zhang, Y., Liiv, T., Shen, K., Zi, B., Zhu, Z., Liu, Q.: Highly selective and sensitive methanol gas sensor based on molecular imprinted silver doped $LaFeO_3$ core–shell and cage structures. Nanotechnology **29**, 145503 (2018)
47. Teeramongkonrasmee, A., Sriyudthsak, M.: Methanol and ammonia sensing characteristics of sol–gel derived thin film gas sensor. Sens. Actuators B **66**, 256–259 (2000)
48. Nechita, V., Schoonman, J., Musat, V.: Ethanol and methanol sensing characteristics of Nb-doped TiO_2 porous thin films. Phys. Status Solidi A **209**(1), 153–159 (2012)
49. Koli, P.B., Kapadnis, K.H., Deshpande, U.G.: Methanol gas sensing properties of pervoskite $LaFeO_3$ nanoparticles doped by transition metals Cr^{3+} and Co^{2+}. J. Chem. Pharm. Res. **9**(1), 253–259 (2017)
50. Gao, Y., Kong, Q., Zhang, J., Xi, G.: General fabrication and enhanced VOC gas-sensing properties of hierarchically porous metal oxides. RSC Adv. **7**, 35897–35904 (2017)
51. Gao, Q., Zheng, W.T., Wei, C.D., Lin, H.M.: Methanol-sensing property improvement of mesostructured zinc oxide prepared by the nano casting strategy. J. Nanomater. 263852 (2013). https://doi.org/10.1155/2013/263852